RSC Advances

PAPER

View Article Online
View Journal | View Issue

Cite this: *RSC Adv.*, 2018, **8**, 33256

Synthesis, surface activities, and aggregation behavior of phenyl-containing carboxybetaine surfactants†

Shifeng Gao,[a] Zhaozheng Song,[a] Di Zhu,[a] Fang Lan[a] and Qingzhe Jiang*[ab]

A series of carboxybetaine surfactants, 2-((4-(alkoxy)-3,5-dimethylbenzyl)dimethyl-ammonio)acetate (C_nOBCb, where *n* represents the hydrocarbon chain length of 12, 14, 16 and 18), were synthesized by an efficient and high-yield route for the first time. The surface activities and aggregation behavior of C_nOBCb in aqueous solution were investigated by equilibrium surface tension, interfacial tension, steady-state fluorescence, dynamic light scattering (DLS), cryogenic transmission electron microscopy (cryo-TEM) and negative-staining transmission electron microscopy (TEM) measurements. In comparison with conventional *N*-alkylbetaine surfactants (C_nCb), the C_nOBCb species, with a phenyl group introduced in the hydrophobic tail, exhibited excellent surface activities, including lower critical micelle concentration (cmc), lower surface tension and stronger adsorption tendency at an air/water interface. C_nOBCb also displayed high efficiency in reducing the toluene/water interfacial tension, with C_{12}OBCb achieving an ultralow interfacial tension (10^{-3} mN m^{-1}) at concentrations from 0.2 to 1 mmol dm^{-3}. The fluorescence intensity ratio and the scattering intensity in DLS measurements changed remarkably at concentrations around the cmc. Furthermore, the C_nOBCb species spontaneously formed vesicles above the cmc in aqueous solution, and the size of the aggregates increased with increasing surfactant concentrations. Flooding experiments showed that C_nOBCb could effectively improve oil recovery by 7.85–10.55%.

Received 23rd July 2018
Accepted 19th September 2018

DOI: 10.1039/c8ra06217j

rsc.li/rsc-advances

1. Introduction

Zwitterionic surfactants incorporating both positively and negatively charged hydrophilic headgroups in the same molecule are attracting increasing attention.[1,2] As an important type of zwitterionic surfactant, betaines have a hydrophilic headgroup comprised of a quaternary ammonium group and an anionic group such as carboxylate, sulfonate, sulfate, or phosphate.[3] Betaine-type surfactants possess distinctive physicochemical properties such as high foam stability, skin and eye compatibility, high efficiency in lowering surface tension, and low toxicity,[4] leading to a wide range of applications in enhanced oil recovery,[5–7] detergents,[8,9] cosmetics[2,10] and textile production.[11]

As the geometry of betaine-type surfactants has a significant effect on their physicochemical properties, considerable efforts have been devoted to their structural optimization. Most reported modifications have been focused on varying the hydrophobic tail,[12–15] hydrophilic headgroup,[16–18] and spacer group.[19] Meanwhile, the introduction of a phenyl group into a hydrocarbon chain significantly influences physicochemical properties such as the critical micelle concentration (cmc), surface tension (γ), standard free energy of micellization (ΔG^0_{mic}), and aggregation structures.[20–26] The location of the phenyl group can also affect the size and structure of the micellar aggregates.[27] Thus, incorporating a phenyl group into betaines may results in phenyl-containing betaine-type surfactants with unique properties. For example, Hu *et al.*[28] studied the adsorption behavior of two pairs of novel betaines and found that the benzyl-substituted alkyl betaines exhibited lower cmc values and enhanced efficiency in lowering the surface tension at air/water interface than the corresponding linear surfactants. Further investigation of the interfacial properties of the same set of surfactants *via* molecular dynamics simulations confirmed that benzene ring incorporation could change and fix the order of the alkyl chain to some extent.[29] However, there are few studies on phenyl-containing betaine-type surfactants.[28–31] The syntheses of phenyl-containing betaine-type surfactants reported in literature are time consuming and inefficient. Thus, the development of an efficient method for synthesizing this type surfactant is still desirable. Further, a systematic study of the effects of the phenyl group on the surface activities and aggregation behavior of these surfactants would help provide

[a]State Key Laboratory of Heavy Oil Processing, College of Science, China University of Petroleum, Beijing 102249, PR China. E-mail: song@cup.edu.cn; Tel: +86 1089733372
[b]School of International Trade and Economics, University of International Business and Economics, Beijing 100029, PR China. E-mail: jiangqingzhe@163.com

† Electronic supplementary information (ESI) available. See DOI: 10.1039/c8ra06217j

a full understand of betaine-type surfactants and experimental guidelines for their application.

In this work, we report a novel series of phenyl-containing carboxybetaine surfactants, 2-((4-(alkyoxy)-3,5-dimethylbenzyl) dimethylammonio)acetate (C_nOBCb, where *n* represents hydrocarbon chain length of 12, 14, 16 and 18), synthesized in high yield using a three-step reaction. The surface activities and aggregation behavior of these surfactants in aqueous solution were systematically investigated by equilibrium surface tension, interfacial tension, steady-state fluorescence, dynamic light scattering, cryogenic transmission electron microscopy (cryo-TEM) and negative-staining transmission electron microscopy (TEM) measurements. In addition, the effect of phenyl group incorporation, hydrocarbon chain length, and the surfactant concentration on the adsorption and aggregation behavior was clarified by comparison with *N*-alkylbetaine surfactants (C_nCb).

2. Experimental methods

2.1. Materials

n-Dodecyl bromide (98%), *n*-tetradecyl bromide (98%), *n*-hexadecyl bromide (97%), *n*-octadecyl bromide (97%), 2,6-dimethylphenol (99%) were purchased from Aladdin Co. (China) and used without further purification. *N*,*N*-Dimethylglycine (98%) was supplied by Alfa Aesar (USA). Sodium hydroxide (99%), paraformaldehyde (99%), tetrabutylammonium bromide (TBAB) (99%), calcein (99%), sodium bicarbonate (99%) and zinc chloride (98%) were obtained from Tianjin Huchen chemical plant (China). Lauryl betaine (C_{12}Cb) (90%) was supplied by BEIJING OUHE TECHNOLOGY CO., LED. Crude oil was obtained from Xinjiang Oilfield (China). The viscosity of oil was 15.8 mPa s at 40 °C, and its density was 0.86 g cm^{-3}. All organic solvents were purchased from Beijing Chemical Co. (China) and were of analytical grade. Deionized water was used in all experiments.

2.2. Synthesis

All the surfactants were synthesized according to Scheme 1. ^{1}H and ^{13}C NMR spectra were recorded at 25 °C on a 500 MHz Bruker III AVANCE spectrometer. Chemical shifts were reported in ppm relative to TMS (for ^{1}H, δ 0.00), CD_3OD (for ^{1}H, δ 3.31; for ^{13}C, δ 48.80), and $CDCl_3$ (for ^{1}H, δ 7.26; for ^{13}C, δ 77.00). High-resolution mass spectra analysis was performed on a Bruker APEX_ULTRA_ 9.4 FT-ICR-MS spectrometer. ^{1}H and ^{13}C NMR spectra were provided in the ESI.†

2.2.1. Synthesis of 2-(alkoxy)-1,3-dimethylbenzene (C_nOB). Sodium hydroxide (0.1 mol, 4 g) was slowly added to a solution of 2,6-dimethylphenol (0.1 mol, 12.2 g) in ethanol (20 mL), and the mixture was stirred at 25 °C for 2 h. After heating to 60 °C, *n*-dodecyl, *n*-tetradecyl, *n*-hexadecyl, or *n*-octadecyl bromide (0.1 mol, 25.4–34.3 g) in *N*,*N*-dimethylformamide (30 mL) was added dropwise to the residue, and the resulting mixture was stirred for 6 h. Then the hot mixture was cooled to room temperature and filtered to remove the insoluble inorganic salt. The filtrate was washed with deionized water and dried over anhydrous sodium sulfate. After filtration, the solution was concentrated *in vacuo* and C_nOB was obtained by reduced pressure distillation (188–226 °C, −0.1 MPa) as a colorless liquid.

2.2.1.1. 2-(Dodecyloxy)-1,3-dimethylbenzene (C_{12}OB). Colorless liquid, yield (76%), ^{1}H NMR (500 MHz, $CDCl_3$) δ 0.87–0.91 (t, 3H, ***Asd CH*$_3$**), 1.28–1.38 (m, 16H, –O–CH_2–CH_2–CH_2–**(*CH*$_2$)$_8$**–CH_3), 1.46–1.54 (m, 2H, –O–CH_2–CH_2–***CH*$_2$**–$(CH_2)_8$–CH_3), 1.77–1.84 (m, 2H, –O–CH_2–***CH*$_2$**–CH_2–$(CH_2)_8$–CH_3), 2.28 (s, 6H, Ar–**(*CH*$_3$)$_2$**), 3.74–3.77 (t, 2H, –O–***CH*$_2$**–CH_2–CH_2–$(CH_2)_8$–CH_3), 6.89–6.92 (t, 1H, ***para*-Ar*H***), 6.99–7.01 (d, 2H, ***meta*-Ar*H***). ^{13}C NMR (125 MHz, $CDCl_3$) δ 14.1, 16.2, 22.7, 26.1, 29.3, 29.5, 29.6, 29.6, 29.6, 30.4, 31.9, 72.2, 122.5, 128.6, 130.8, 156.0. 156.2. HRMS (ESI+) *m*/*z*: calcd for $C_{20}H_{35}O^+$ (M + H), 291.2684; found, 291.2682.

2.2.1.2. 2-(Tetradecyloxy)-1,3-dimethylbenzene (C_{14}OB). Colorless liquid, yield (79%), ^{1}H NMR (500 MHz, $CDCl_3$) δ 0.88–0.91 (t, 3H, –***CH*$_3$**), 1.28–1.37 (m, 20H, –O–CH_2–CH_2–CH_2 –**(*CH*$_2$)$_{10}$**–CH_3), 1.47–1.53 (m, 2H, –O–CH_2–CH_2–***CH*$_2$**–$(CH_2)_{10}$–CH_3), 1.78–1.84 (m, 2H, –O–CH_2–***CH*$_2$**–CH_2–$(CH_2)_{10}$–CH_3), 2.28 (s, 6H, Ar–**(*CH*$_3$)$_2$**), 3.75–3.77 (t, 2H, –O–***CH*$_2$**–CH_2–CH_2–$(CH_2)_{10}$–CH_3), 6.89–6.92 (t, 1H, ***para*-Ar*H***), 7.00–7.01 (d, 2H, ***meta*-Ar*H***). ^{13}C NMR (125 MHz, $CDCl_3$) δ 14.1, 16.2, 22.7, 26.1, 29.3, 29.5, 29.6, 29.6, 29.6, 29.7, 30.4, 31.9, 72.2, 123.5, 128.7, 130.9, 156.0. 156.2. HRMS (ESI+) *m*/*z*: calcd for $C_{22}H_{39}O^+$ (M + H), 319.2295; found, 319.2296.

2.2.1.3. 2-(Hexadecyloxy)-1,3-dimethylbenzene (C_{16}OB). White solid, yield (74%), ^{1}H NMR (500 MHz, $CDCl_3$) δ 0.88–0.91 (t, 3H, –***CH*$_3$**), 1.28–1.38 (m, 24H, –O–CH_2–CH_2–CH_2–**(*CH*$_2$)$_{12}$**–CH_3), 1.48–1.54 (m, 2H, –O–CH_2–CH_2–***CH*$_2$**–$(CH_2)_{12}$–CH_3), 1.78–1.84 (m, 2H, –O–CH_2–***CH*$_2$**–CH_2–$(CH_2)_{12}$–CH_3), 2.29 (s, 6H, Ar–**(*CH*$_3$)$_2$**), 3.75–3.78 (t, 2H, –O–***CH*$_2$**–CH_2–CH_2–$(CH_2)_{10}$–CH_3), 6.90–6.93 (t, 1H, ***para*-Ar*H***), 7.00–7.02 (d, 2H, ***meta*-Ar*H***). ^{13}C NMR (125 MHz, $CDCl_3$) δ 14.1, 16.2, 22.7, 26.1, 29.3, 29.5, 29.6, 29.6, 29.6, 29.7, 30.4, 31.9, 72.2, 123.5, 128.7, 130.9, 156.0. 156.2. HRMS (ESI+) *m*/*z*: calcd for $C_{24}H_{43}O^+$ (M + H), 347.3308; found, 347.3310.

2.2.1.4. 2-(Octadecyloxy)-1,3-dimethylbenzene (C_{18}OB). White solid, yield (73%), ^{1}H NMR (500 MHz, $CDCl_3$) δ 0.87–0.90 (t, 3H, –***CH*$_3$**), 1.27–1.38 (m, 28H, –O–CH_2–CH_2–CH_2–**(*CH*$_2$)$_{14}$**–CH_3), 1.47–1.53 (m, 2H, –O–CH_2–CH_2 –***CH*$_2$**–$(CH_2)_{14}$–CH_3), 1.78–1.83 (m, 2H, –O–CH_2–***CH*$_2$**–CH_2–$(CH_2)_{14}$–CH_3), 2.28 (s, 6H, Ar–**(*CH*$_3$)$_2$**), 3.74–3.77 (t, 2H, –O–***CH*$_2$**–CH_2–CH_2–$(CH_2)_{10}$–CH_3), 6.89–6.92 (t, 1H, ***para*-Ar*H***), 7.00–7.01 (d, 2H, ***meta*-Ar*H***). ^{13}C NMR (125 MHz, $CDCl_3$) δ 14.1, 16.2, 22.6, 26.1, 29.3, 29.5, 29.6, 29.6, 29.6, 29.7, 30.4, 31.9, 72.2, 123.5, 128.7, 130.9, 156.0. 156.2. HRMS (ESI+) *m*/*z*: calcd for $C_{26}H_{47}O^+$ (M + H), 375.3620; found, 375.3621.

2.2.2. Synthesis of 5-(chloromethy)-2-(alkoxy)-1,3-dimethylbenzene (C_nOBMCl). Acetic acid (20 mL) and TBAB (0.005 mol, 1.6 g) were added to a stirred solution of C_nOB (0.1 mol, 29.1–37.3 g) dissolved in approximately 30 mL of *n*-hexane. Then, dry hydrogen chloride gas was continuously bubbled through the solution at room temperature. After increasing the temperature to 70 °C, zinc chloride (0.1 mol, 13.6 g) and paraformaldehyde (0.1 mol, 3 g) were slowly added, and the resulting mixture was refluxed for 8 h. The upper organic phase was separated, washed with deionized water, and then

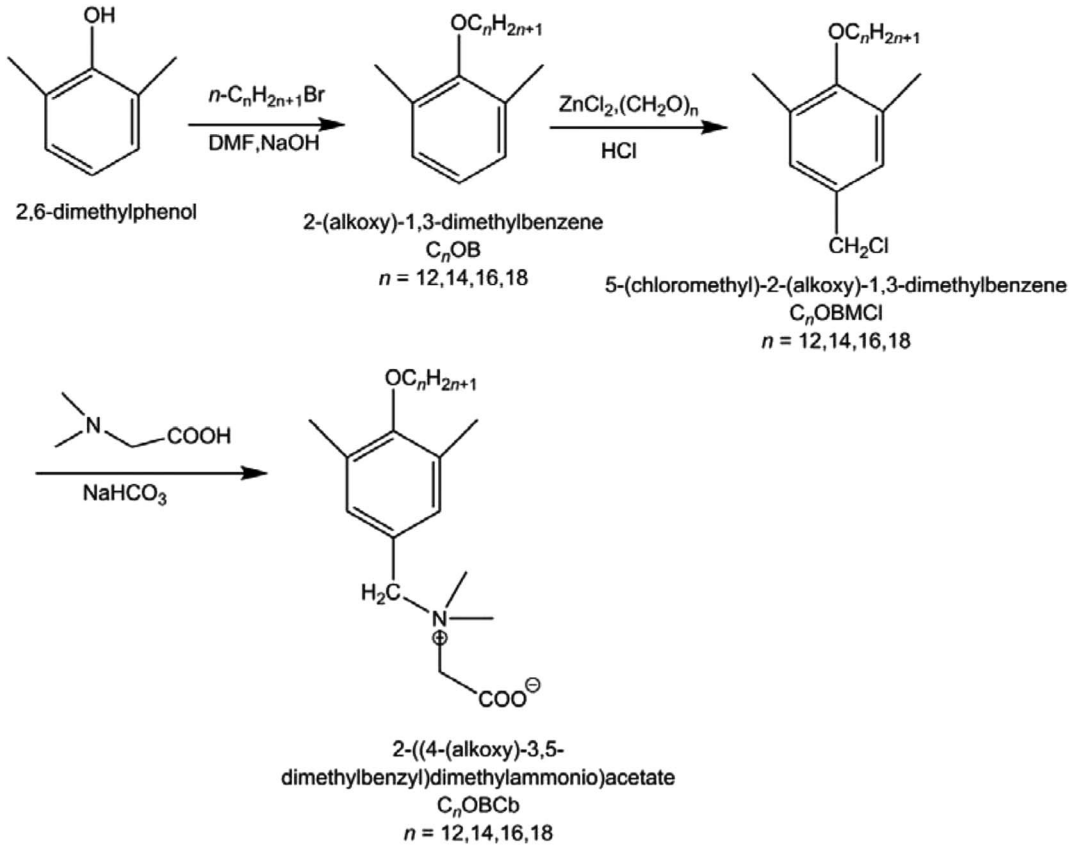

Scheme 1 Synthesis route of C_nOBCb (n = 12, 14, 16, 18).

dried over anhydrous sodium sulfate. After filtration, the filtrate was concentrated under reduced pressure and C_nOBMCl was purified by flash column chromatography using petroleum ether and ethyl acetate = 20 : 1 as the eluent.

2.2.2.1. 5-(Chloromethy)-2-(dodecyloxy)-1,3-dimethylbenzene (C_{12}OBMCl). White solid, yield (82%), ^{1}H NMR (500 MHz, $CDCl_3$) δ 0.87–0.90 (t, 3H, –***CH*$_3$**), 1.27–1.36 (m, 16H, –O–CH_2–CH_2–CH_2–**(*CH*$_2$)$_8$**–CH_3), 1.46–1.52 (m, 2H, –O–CH_2–CH_2–***CH*$_2$**–$(CH_2)_8$–CH_3), 1.76–1.82 (m, 2H, –O–CH_2–***CH*$_2$**–CH_2–$(CH_2)_8$–CH_3), 2.27 (s, 6H, Ar–**(*CH*$_3$)$_2$**), 3.73–3.75 (t, 2H, –O–***CH*$_2$**–CH_2–CH_2–$(CH_2)_8$–CH_3), 4.50 (s, 2H, ***para***-Ar–***CH*$_2$**Cl), 7.03 (s, 2H, ***meta***-Ar***H***). ^{13}C NMR (125 MHz, $CDCl_3$) δ 14.1, 16.2, 22.6, 26.1, 29.5, 29.6, 29.6, 29.6, 30.3, 31.9, 46.3, 72.3, 129.1, 131.4, 132.4, 156.2. HRMS (ESI+) m/z: calcd for $C_{21}H_{35}O^+$ (M − Cl), 303.2682; found, 303.2685.

2.2.2.2. 5-(Chloromethy)-2-(tetradecyloxy)-1,3-dimethylbenzene (C_{14}OBMCl). White solid, yield (77%), ^{1}H NMR (500 MHz, $CDCl_3$) δ 0.87–0.90 (t, 3H, –***CH*$_3$**), 1.27–1.36 (m, 16H, –O–CH_2–CH_2–CH_2–**(*CH*$_2$)$_{10}$**–CH_3), 1.46–1.52 (m, 2H, –O–CH_2–CH_2–***CH*$_2$**–$(CH_2)_{10}$–CH_3), 1.76–1.82 (m, 2H, –O–CH_2–***CH*$_2$**–CH_2–$(CH_2)_{10}$–CH_3), 2.27 (s, 6H, Ar–**(*CH*$_3$)$_2$**), 3.73–3.75 (t, 2H, –O–***CH*$_2$**–CH_2–CH_2–$(CH_2)_{10}$–CH_3), 4.50 (s, 2H, ***para***-Ar–***CH*$_2$**Cl), 7.03 (s, 2H, ***meta***-Ar***H***). ^{13}C NMR (125 MHz, $CDCl_3$) δ 14.1, 16.2, 22.6, 26.1, 29.3, 29.5, 29.6, 29.6, 29.6, 29.6, 30.3, 31.9, 46.3, 72.3, 129.1, 131.3, 132.4, 156.2. HRMS (ESI+) m/z: calcd for $C_{23}H_{39}O^+$ (M − Cl), 331.2995; found, 331.2997.

2.2.2.3. 5-(Chloromethy)-2-(hexadecyloxy)-1,3-dimethylbenzene (C_{16}OBMCl). White solid, yield (81%), ^{1}H NMR (500 MHz, $CDCl_3$) δ 0.87–0.90 (t, 3H, –***CH*$_3$**), 1.27–1.36 (m, 16H, –O–CH_2–CH_2–CH_2–**(*CH*$_2$)$_{12}$**–CH_3), 1.46–1.52 (m, 2H, –O–CH_2–CH_2–***CH*$_2$**–$(CH_2)_{12}$–CH_3), 1.76–1.82 (m, 2H, –O–CH_2–***CH*$_2$**–CH_2–$(CH_2)_{12}$–CH_3), 2.27 (s, 6H, Ar–**(*CH*$_3$)$_2$**), 3.73–3.75 (t, 2H, –O–***CH*$_2$**–CH_2–CH_2–$(CH_2)_{12}$–CH_3), 4.50 (s, 2H, ***para***-Ar–***CH*$_2$**Cl), 7.03 (s, 2H, ***meta***-Ar***H***). ^{13}C NMR (125 MHz, $CDCl_3$) δ 14.1, 16.2, 22.6, 26.1, 29.3, 29.5, 29.6, 29.6, 29.6, 29.6, 29.6, 30.3, 31.9, 46.3, 72.3, 129.1, 131.4, 132.4, 156.2. HRMS (ESI+) m/z: calcd for $C_{25}H_{43}O^+$ (M − Cl), 359.3308; found, 359.3308.

2.2.2.4. 5-(Chloromethy)-2-(octadecyloxy)-1,3-dimethylbenzene (C_{18}OBMCl). White solid, yield (75%), ^{1}H NMR (500 MHz, $CDCl_3$) δ 0.87–0.90 (t, 3H, –***CH*$_3$**), 1.27–1.36 (m, 16H, –O–CH_2–CH_2–CH_2–**(*CH*$_2$)$_{14}$**–CH_3), 1.46–1.52 (m, 2H, –O–CH_2–CH_2–***CH*$_2$**–$(CH_2)_{14}$–CH_3), 1.76–1.82 (m, 2H, –O–CH_2–***CH*$_2$**–CH_2–$(CH_2)_{14}$–CH_3), 2.27 (s, 6H, Ar–**(*CH*$_3$)$_2$**), 3.73–3.75 (t, 2H, –O–***CH*$_2$**–CH_2–CH_2–$(CH_2)_{14}$–CH_3), 4.50 (s, 2H, ***para***-Ar–***CH*$_2$**Cl), 7.03 (s, 2H, ***meta***-Ar***H***). ^{13}C NMR (125 MHz, $CDCl_3$) δ 14.1, 16.2, 22.6, 26.1, 29.3, 29.5, 29.5, 29.6, 29.6, 29.6, 29.6, 30.3, 31.9, 46.2, 72.3, 129.1, 131.4, 132.4, 156.2. HRMS (ESI+) m/z: calcd for $C_{27}H_{47}O^+$ (M − Cl), 387.3621; found, 387.3620.

2.2.3. Synthesis of C_nOBCb. Sodium bicarbonate (0.02 mol, 1.68 g) was slowly added to a solution of *N*,*N*-dimethylglycine (0.02 mol, 2.06 g) in 40 mL of ethanol at 80 °C and stirred for approximately 1 h. C_nOBMCl (0.02 mol, 6.76–8.44 g) dissolved in

15 mL of *n*-hexane was added dropwise into this solution, and the mixture was refluxed for 6 h. After all solvent was evaporated, the resulting waxy crude betaine surfactant was extracted with 20 mL of ethanol. The extract was evaporated to dryness and repeatedly recrystallized from a mixture of methanol and acetone. The product was then dried at 60 °C under vacuum.

2.2.3.1. 2-((4-(Dodecyloxy)-3,5-dimethylbenzyl)dimethylammonio) acetate (C_{12}OBCb). White solid, yield (85%), ^{1}H NMR (500 MHz, $CDCl_3$) δ 0.89–0.91 (t, 3H, –***CH*$_3$**), 1.30–1.40 (m, 16H, –O–CH_2–CH_2–CH_2–**(*CH*$_2$)$_8$**–CH_3), 1.51–1.57 (m, 2H, –O–CH_2–CH_2–***CH*$_2$**–$(CH_2)_8$–CH_3), 1.78–1.84 (m, 2H, –O–CH_2–***CH*$_2$**–CH_2–$(CH_2)_8$–CH_3), 2.30 (s, 6H, Ar–***CH*$_3$**), 3.19 (s, 6H, –CH_2–N–**(*CH*$_3$)$_2$**–CH_2–COO^-), 3.64 (s, 3H, –CH_2–N–$(CH_3)_2$–***CH*$_2$**–COO^-), 3.79–3.82 (t, 2H, –O–***CH*$_2$**–CH_2–CH_2–$(CH_2)_8$–CH_3), 4.67 (s, 2H, Ar–***CH*$_2$**–$N^+(CH_3)_2$–CH_2–), 7.19 (s, 2H, ***meta*-Ar*H***). ^{13}C NMR (125 MHz, $CDCl_3$) δ 14.2, 16.2, 22.6, 27.0, 30.2, 30.4, 30.5, 30.5, 30.5, 31.2, 32.8, 51.0, 63.7, 67.3, 73.2, 124.2, 133.0, 134.3, 159.1, 168.8. HRMS (ESI+) *m*/*z*: calcd for $C_{25}H_{43}NO_3^+$ (M + H), 406.3315; found, 406.3309.

2.2.3.2. 2-((4-(Tetradecyloxy)-3,5-dimethylbenzyl)dimethylammonio) acetate (C_{14}OB Cb). White solid, yield (91%), ^{1}H NMR (500 MHz, $CDCl_3$) δ 0.88–0.91 (t, 3H, –***CH*$_3$**), 1.30–1.40 (m, 20H, –O–CH_2–CH_2–CH_2–**(*CH*$_2$)$_{10}$**–CH_3), 1.51–1.57 (m, 2H, –O–CH_2–CH_2–***CH*$_2$**–$(CH_2)_{10}$–CH_3), 1.78–1.84 (m, 2H, –O–CH_2–***CH*$_2$**–CH_2–$(CH_2)_{10}$–CH_3), 2.30 (s, 6H, Ar–***CH*$_3$**), 3.19 (s, 6H, –CH_2–N–**(*CH*$_3$)$_2$**–CH_2–COO^-), 3.64 (s, 3H, –CH_2–N–$(CH_3)_2$–***CH*$_2$**–COO^-), 3.79–3.81 (t, 2H, –O–***CH*$_2$**–CH_2–CH_2–$(CH_2)_{10}$–CH_3), 4.67 (s, 2H, Ar–***CH*$_2$**–$N^+(CH_3)_2$–CH_2–), 7.19 (s, 2H, ***meta*-Ar*H***). ^{13}C NMR (125 MHz, $CDCl_3$) δ 14.2, 16.2, 23.5, 27.0, 30.2, 30.4, 30.5, 30.5, 30.5, 30.6, 31.2, 32.8, 51.0, 63.7, 67.3, 73.2, 124.2, 133.0, 134.3, 159.1, 168.8. HRMS (ESI+) *m*/*z*: calcd for $C_{27}H_{47}NO_3^+$ (M + H), 434.3628; found, 434.3630.

2.2.3.3. 2-((4-(Hexadecyloxy)-3,5-dimethylbenzyl)dimethylammonio) acetate (C_{16}OB Cb). White solid, yield (88%), ^{1}H NMR (500 MHz, $CDCl_3$) δ 0.88–0.91 (t, 3H, –***CH*$_3$**), 1.29–1.41 (m, 24H, –O–CH_2–CH_2–CH_2–**(*CH*$_2$)$_{12}$**–CH_3), 1.51–1.57 (m, 2H, –O–CH_2–CH_2–***CH*$_2$**–$(CH_2)_{12}$–CH_3), 1.78–1.84 (m, 2H, –O–CH_2–***CH*$_2$**–CH_2–$(CH_2)_{12}$–CH_3), 2.29 (s, 6H, Ar–***CH*$_3$**), 3.18 (s, 6H, –CH_2–N–**(*CH*$_3$)$_2$**–CH_2–COO^-), 3.64 (s, 3H, –CH_2–N–$(CH_3)_2$–***CH*$_2$**–COO^-), 3.79–3.81 (t, 2H, –O–***CH*$_2$**–CH_2–CH_2–$(CH_2)_{12}$–CH_3), 4.67 (s, 2H, Ar–***CH*$_2$**–$N^+(CH_3)_2$–CH_2–), 7.18 (s, 2H, ***meta*-Ar*H***). ^{13}C NMR (125 MHz, $CDCl_3$) δ 14.2, 16.2, 23.5, 27.0, 30.2, 30.4, 30.5, 30.5, 30.5, 30.6, 31.2, 32.8, 51.0, 63.7, 67.3, 73.2, 124.2, 133.0, 134.3, 159.1, 168.8. HRMS (ESI+) *m*/*z*: calcd for $C_{29}H_{51}NO_3^+$ (M + H), 462.3941; found, 462.3942.

2.2.3.4. 2-((4-(Octadecyloxy)-3,5-dimethylbenzyl)dimethylammonio) acetate (C_{18}OB Cb). White solid, yield (83%), ^{1}H NMR (500 MHz, $CDCl_3$) δ 0.88–0.91 (t, 3H, –***CH*$_3$**), 1.29–1.40 (m, 28H, –O–CH_2–CH_2–CH_2–**(*CH*$_2$)$_{14}$**–CH_3), 1.51–1.57 (m, 2H, –O–CH_2–CH_2–***CH*$_2$**–$(CH_2)_{14}$–CH_3), 1.78–1.84 (m, 2H, –O–CH_2–***CH*$_2$**–CH_2–$(CH_2)_{14}$–CH_3), 2.30 (s, 6H, Ar–***CH*$_3$**), 3.18 (s, 6H, –CH_2–N–**(*CH*$_3$)$_2$**–CH_2–COO^-), 3.64 (s, 3H, –CH_2–N–$(CH_3)_2$–***CH*$_2$**–COO^-), 3.79–3.81 (t, 2H, –O–***CH*$_2$**–CH_2–CH_2–$(CH_2)_{14}$–CH_3), 4.67 (s, 2H, Ar–***CH*$_2$**–$N^+(CH_3)_2$–CH_2–), 7.18 (s, 2H, ***meta*-Ar*H***). ^{13}C NMR (125 MHz, $CDCl_3$) δ 14.2, 16.3, 23.5, 27.0, 30.3, 30.4, 30.5, 30.5, 30.5, 30.6, 31.2, 32.8, 51.0, 63.7, 67.3, 73.2, 124.2, 133.0, 134.3, 159.1, 168.7. HRMS (ESI+) *m*/*z*: calcd for $C_{31}H_{55}NO_3^+$ (M + H), 490.4254; found, 490.4258.

2.3. Measurements

2.3.1. Thermal stability measurements. The thermostability of C_nOBCb (n = 12, 14, 16, or 18) was investigated using a HTG–3 thermogravimetric analyzer (Beijing Henven Scientific Instrument Factory, China). The sample was heated from 10 to 600 °C with a heating rate of 10 °C min^{-1} in a nitrogen atmosphere at a flow rate of 50 mL min^{-1}.

2.3.2. Surface tension measurements. The surface tensions of aqueous surfactant solutions were measured with a BZY–2 automatic tensiometer by using the Wilhelmy plate technique at 25.0 ± 0.1 °C. To obtain equilibrium surface tension, sets of measurements were taken until the change in surface tension was less than 0.01 mN m^{-1} every 3 min. The cmc and surface tension at the cmc (γ_{cmc}) were determined from the break point of the surface tension and the logarithm of the concentration curve (γ − log C), respectively. The adsorption amount of surfactant Γ was calculated according to the Gibbs adsorption isotherm equation:[32]

$$\Gamma = -\frac{1}{2.303nRT}\left(\frac{d\gamma}{d\log C}\right). \quad (1)$$

where γ is the surface tension in mN m^{-1}, Γ is the adsorbed amount in mol m^{-2}, R is the gas constant (8.314 J mol^{-1} K^{-1}), T is the absolute temperature in K, C is the surfactant concentration, and (dγ/d log C) is the slope below the cmc in the surface tension plot. The value of n, which dependents theoretically on the surfactant type and structure, is taken as 1 for a zwitterionic surfactant in aqueous solution.[33] The occupied area per surfactant molecule at the cmc, A_{cmc} (nm^2), is obtained from the saturation adsorption (Γ_{cmc}) using the following equation:

$$A_{cmc} = \frac{1}{N\Gamma_{cmc}}. \quad (2)$$

where N is Avogadro's number (6.022 × 10^{23} mol^{-1}) and, Γ_{cmc} is the surface excess concentration at the cmc.

2.3.3. Interfacial tension measurements. The interfacial tension between toluene (or *n*-heptane) and aqueous surfactant solution was measured using a TX–500C spinning drop interfacial tension meter (Shanghai Zhongchen, China) at 25.0 ± 0.1 °C. The rotation speed was set at 12 rps in all measurements. Interfacial tension values were recorded until equilibrium was reached.

2.3.4. Steady-state fluorescence measurements. The fluorescence measurements were performed using a RF5301 fluorescence spectrophotometer (Shimadzu Corporation, Japan). The spectra were recorded between 350 and 500 nm with an excitation wavelength of 335 nm, and the excitation and emission slit widths were fixed at 3.0 nm. The concentration of pyrene in each solution was 1 × 10^{-6} mol dm^{-3}. The fluorescence intensity ratio of the first to the third vibronic peaks, I_1/I_3, were used to estimate the micropolarity in its solubilization site.[34]

2.3.5. Dynamic light scattering (DLS). DLS measurements were performed with a Nano ZS Zetasizer (Malvern Instruments Laboratory, UK) equipped with a Helium–Neon laser source operating at λ_o = 632.8 nm. The scattering intensity was measured at an angle of 173° to the incident beam. The auto-correlation function was analyzed using the CONTIN method. The apparent hydrodynamic diameter (D_h) was obtained according to the Stokes–Einstein equation,[25,27] $D_h = kT/(3\pi\eta D)$, where D is the diffusion coefficient, k is the Boltzmann constant, T is the absolute temperature, and η is the viscosity of the solution. All sample solutions were filtered through a 0.45 μm membrane filter and measured three times at 25 °C.

2.3.6. Transmission electron microscopy (TEM). TEM measurements were performed on a JEM–2100 transmission electron microscope (JEOL Ltd., Japan) at an accelerating voltage of 200 kV. The TEM samples were prepared using the negative-staining method with phosphotungstic acid aqueous solution (2%). A droplet of the sample solution was spread on a 300-mesh copper grid coated with a Formvar film, and excess sample solution was wicked away with a piece of filter paper. When the grid was partially dried, a drop of staining solution was added onto the grid over 10 min. After drying, the morphologies of the samples were examined by TEM.

2.3.7. Core flooding experiment. Surfactant flooding experiments were performed in the artificial sandstone core at the oil reservoir temperature of 40 °C. To begin with, the porosity and permeability of the sandstone core were determined using an Automated Permeameter–Porosimeter (Coretest systems, Inc., U.S.A), and the basic parameters of sandstone core were given in Table 3. The core plug was loaded into the core holder and vacuumed for 2 h. After the core was saturated with formation brine (the composition of brine was listed in Table S2†), the crude oil was injected into core plug until the water cut reached less than 1%. After that, the core was aged in the core holder for 24 h and water flooding was conducted at a flow rate of 0.4 mL min^{-1} until the water cut reached 98%. Finally, 0.3 PV surfactant slug was injected into the core after water flooding and then subsequent water flooding was conducted until water cut reached 98%. The produced fluid was collected using a measuring cylinder to record the oil and water production.

3. Results and discussion

3.1. Thermogravimetric analysis (TGA)

The thermostability of C_nOBCb (n = 12, 14, 16, or 18) was determined through TGA to evaluate the temperature range in which these surfactants can be applied. The TGA curves of C_nOBCb are shown in Fig. 1. The results show that the weight of C_nOBCb remains essentially unchanged below 200 °C. As the temperature increases, the compounds gradually decompose and then totally break down at approximately 500 °C. These findings indicate that C_nOBCb (n = 12, 14, 16, or 18) exhibit excellent thermostability and can be utilized at temperatures up to 200 °C. Additionally, changing the hydrocarbon chain length did not significantly affect the onset temperature of thermal decomposition. It is also worth mentioning that the thermal

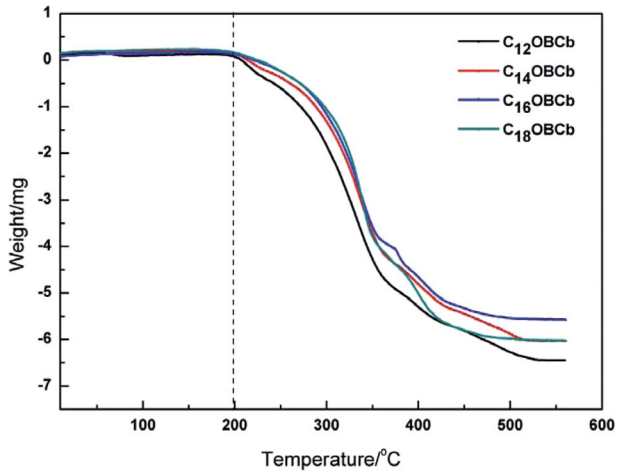

Fig. 1 TGA curves of C_nOBCb.

decomposition temperatures of C_nOBCb are higher than that of *N*-dodecyl-*N*,*N*-dimethyl-2-ammonio-1-ethanecarbonate (C_{12}Cb, $C_{12}H_{25}N^+(CH_3)_2CH_2COO^-$; 160 °C).[35] Thus, C_{12}OBCb shows better thermal stability than the corresponding linear betaine-type surfactants and the introduction of a phenyl group in the surfactant molecule can significantly increase the thermal stability of betaine-type surfactants.

3.2. Equilibrium surface tension

The surface tension is plotted as a function of concentration of C_nOBCb (n = 12, 14, 16, or 18) in Fig. 2. The surface tension of C_nOBCb initially decreases as the surfactant concentration increases, and then reaches an equilibrium value. The break points of the curves were taken as cmc values. The cmc, γ_{cmc}, Γ_{cmc}, and A_{cmc} values of C_nOBCb are listed in Table 1, along with the data for C_nCb ($C_nH_{2n+1}N^+(CH_3)_2$–CH_2COO^-) for comparison.[36] The variation of the cmc with the hydrocarbon chain length for homologous straight-chain ionic surfactants can be described by the empirical Klevens equation[37] as follows:

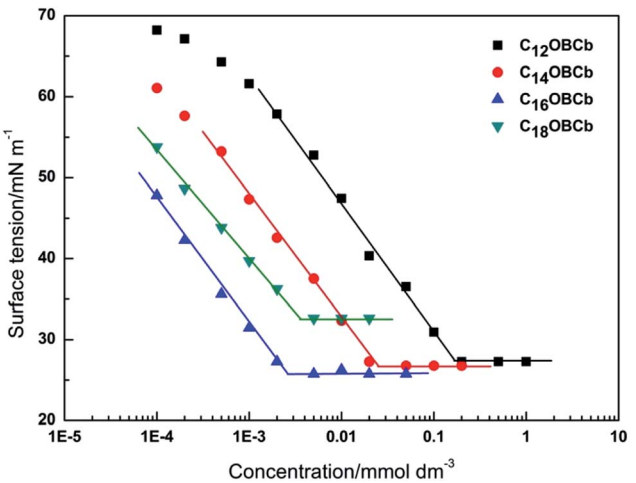

Fig. 2 Variation of the surface tension with the surfactant concentration for C_nOBCb at 25 °C.

Table 1 Surface activity parameters of carboxyl betaine surfactants C_nOBCb

Surfactant	cmc (mmol dm^{-3})	γ_{cmc} (mN m^{-1})	$10^6\ \Gamma_{cmc}$ (mol m^{-2})	A_{cmc} (nm^2)
$C_{12}OBCb$	0.1881	27.3	2.63	0.63
$C_{14}OBCb$	0.0229	26.7	2.66	0.62
$C_{16}OBCb$	0.0023	25.6	2.76	0.60
$C_{18}OBCb$	0.0035	32.6	2.33	0.71
$C_{12}H_{25}N^+(CH_3)_2CH_2COO^-$	1.8	36.5	3.57	0.47
$C_{14}H_{29}N^+(CH_3)_2CH_2COO^-$	0.18	37.5	3.55	0.47
$C_{16}H_{33}N^+(CH_3)_2CH_2COO^-$	0.02	39.7	4.13	0.40

$$\log \text{cmc} = A - Bn \quad (3)$$

where n is the number of carbon atoms in the hydrocarbon chain. The A value is a constant for a particular ionic head at a given temperature, whereas the B value is close to 0.3 for anionic and cationic surfactants and 0.5 for zwitterionic and nonionic surfactants. The relationships between the cmc and the hydrocarbon chain length of C_nOBCb and C_nCb are plotted in Fig. 3. For the C_nCb series, the logarithm of the cmc decreases linearly as the hydrocarbon chain length increases. However, for C_nOBCb, a similar trend is observed for hydrocarbon chain lengths of 12–16 and a deviation from linearity occurs when the hydrocarbon chain length reaches 18. This phenomenon has also been observed in some gemini zwitterionic surfactants.[38,39] A reasonable explanation, as reported by Mukerjee,[40] is that the cmc only changes slightly as the hydrocarbon chain length increases up to 18 because the long hydrocarbon chains coil in aqueous solution. The B value of C_nOBCb with hydrocarbon chain lengths from 12 to 16 is determined as 0.47, which is close to those for zwitterionic betaine surfactants such as sulfobetaine-type surfactants (C_nSb; $B = 0.48$)[41] and C_nCb ($B = 0.49$).[36] It is also noteworthy that the cmc values of C_nOBCb ($n = 12$, 14, or 16) are approximately one order of magnitude lower than those of C_nCb with the same hydrocarbon chain lengths. Thus, the phenyl-containing C_n-OBCb surfactants have a better micellization ability at relatively low concentrations. This behavior is attributed to an enhancement of hydrophobic interactions caused by the introduction of a phenyl group near the headgroup.[25,42]

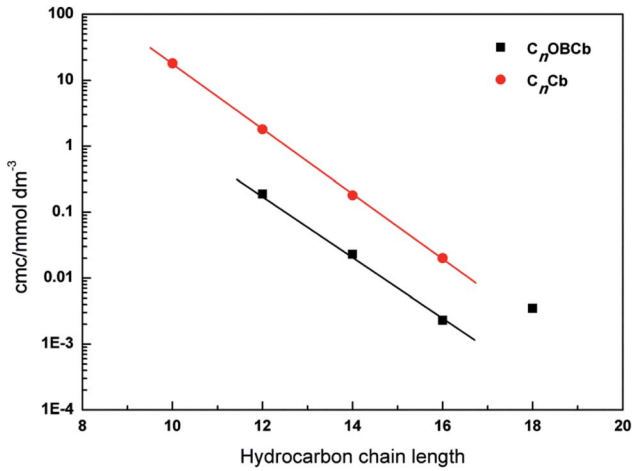

Fig. 3 Relationship between the cmc and hydrocarbon chain length for C_nOBCb and N-alkylbetaine surfactants C_nCb.

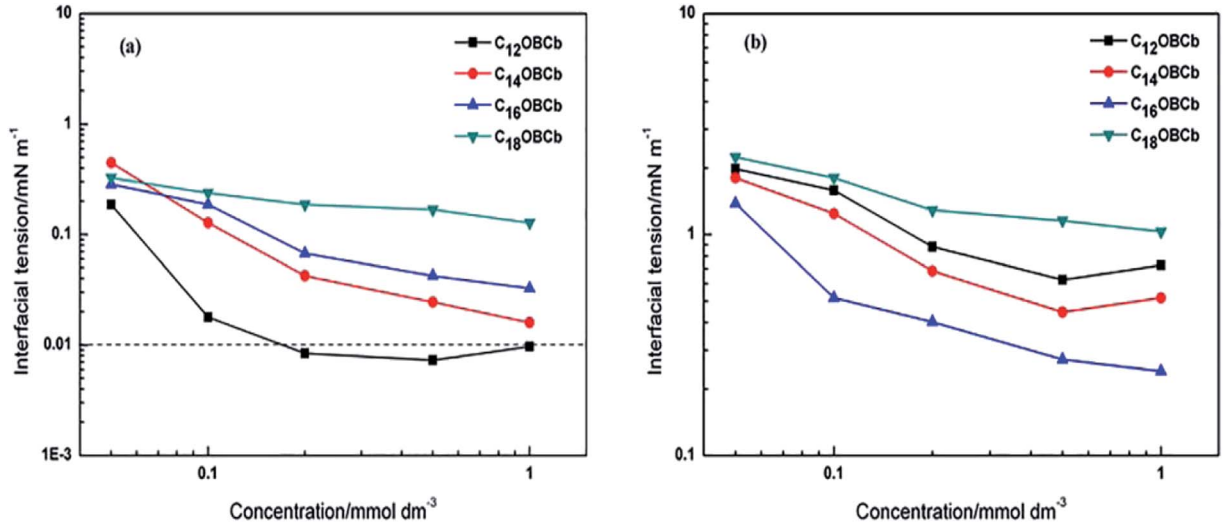

Fig. 4 Variation of the interfacial tension with C_nOBCb concentration against toluene (a) and n-heptane (b) at 25 °C.

Table 2 Parameters on micellization and adsorption of carboxyl betaine surfactants C_nOBCb

Surfactant	pC_{20}	cmc/C_{20}	ΔG^0_{mic} (kJ mol^{-1})	ΔG^0_{ads} (kJ mol^{-1})
C_{12}OBCb	5.13	25.4	−31.20	−46.82
C_{14}OBCb	6.06	26.3	−36.42	−52.03
C_{16}OBCb	7.07	27.1	−42.12	−57.60
C_{18}OBCb	6.63	15.1	−41.08	−56.40
$C_{12}H_{25}N^+(CH_3)_2CH_2COO^-$	3.91	6.5	—	—
$C_{14}H_{29}N^+(CH_3)_2CH_2COO^-$	4.62	7.5	—	—
$C_{16}H_{33}N^+(CH_3)_2CH_2COO^-$	5.54	6.9	—	—

For $n = 12$, 14, and 16, the γ_{cmc} values of C_nOBCb are much smaller than those of C_nCb (36.5–39.7 mN m^{-1} at 23 °C), indicating that C_nOBCb has a greater efficiency in lowering the surface tension of water than C_nCb. Meanwhile, the γ_{cmc} values of C_nOBCb decrease on increasing the hydrocarbon chain length from 12 to 16. However, for $n = 18$, the γ_{cmc} value is 32.63 mN m^{-1}, which is slightly larger than those of other homogeneous surfactants. This aberrant behavior has also been observed for ultra-long unsaturated amidobetaine surfactants,[43] cationic gemini surfactants,[39,44] and zwitterionic heterogemini surfactants.[22] This phenomenon can be attributed to the fact that a long hydrophobic chain ($n = 18$) increase the steric hindrance between surfactant molecules, which makes surfactant molecules prone to forming premicellar aggregates in aqueous solution rather than adsorbing at the air/water interface.[43]

3.3. Interfacial tension measurements

The interfacial tension as a function of C_nOBCb concentration in the range of 0.05–1 mmol dm^{-3} against toluene and *n*-heptane are illustrated in Fig. 4(a) and (b), respectively. The C_nOBCb surfactants exhibit similar trends against both toluene and *n*-heptane, that is, the interfacial tensions decrease almost linearly with increasing surfactant concentrations in the investigated range. For the toluene/water interface, C_{12}OBCb exhibits the lowest interfacial tension among the C_nOBCb species, reaching an ultralow value of 10^{-3} mN m^{-1} in the concentration range of 0.2–1 mmol dm^{-3}, which indicates excellent interfacial activity. For the *n*-heptane/water interface, C_{16}OBCb exhibits the lowest interfacial tension, reaching a value of 0.24 mN m^{-1} at 1 mmol dm^{-3} (Fig. 4(b)). For both the toluene/water and *n*-heptane/water interfaces, C_{18}OBCb shows the lowest capability for reducing the interfacial tension. This behavior is probably due to the longer hydrophobic chains in C_{18}OBCb being prone to curl, leading to a loose arrangement of molecules at the interface. Thus, the concentration of effective surfactant molecules decreases in comparison with those of other homogenous C_nOBCb species. Interestingly, it is noted that the interfacial tension values in toluene/water for C_nOBCb

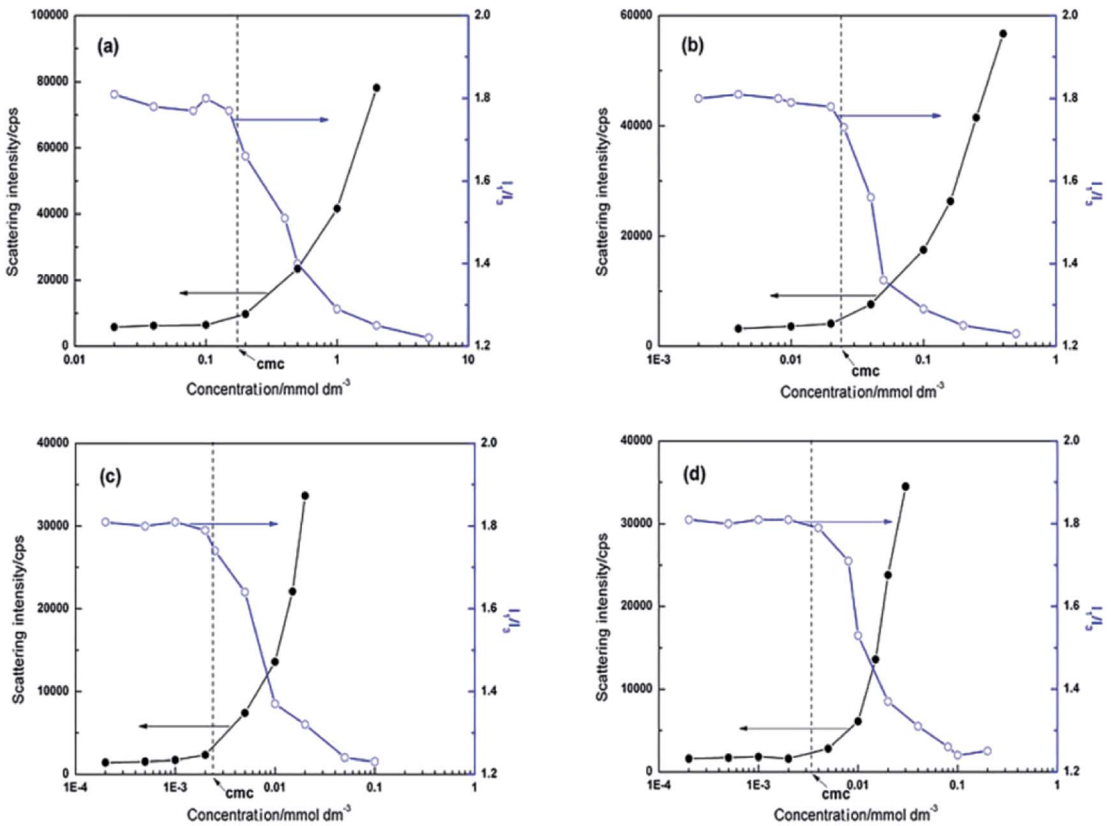

Fig. 5 Variation of the pyrene fluorescence intensity ratio I_1/I_3 and scattering intensity by DLS with the surfactant concentration for C_nOBCb: n = (a) 12, (b) 14, (c) 16, (d) 18.

($n = 12$, 14, 16, or 18) are lower than those in *n*-heptane/water at the same concentrations. It can be deduced that the C_nOBCb surfactants exhibit much higher efficiency in reducing interfacial tension against arenes than *n*-alkanes with the same number of carbon atoms in the molecular structure.

3.4. Adsorption properties

The A_{cmc}, which is closely correlated with the Γ_{cmc}, can provide information about the orientation and packing degree of surfactant molecules at the air/water interface. The A_{cmc} values of C_nOBCb, listed in Table 1, range from 0.60 to 0.71 nm^2, which are slightly larger than those of C_nCb.[36] This difference may be caused by the bulky phenyl group within the hydrophobic tail. Meanwhile, the A_{cmc} values decrease marginally on increasing the hydrocarbon chain length from 12 to 16, and then increase abruptly for $n = 18$. The initial decrease of A_{cmc} reflects that tight packing of C_nOBCb molecules at the air/water interface owing to the enhancement of hydrophobic interactions between the hydrocarbon chains. It seems that the presence of a rigid phenyl group in the hydrophobic tail favors an extended orientation of the hydrophobic chain, resulting in close packing of the surfactant molecules at the air/water interface.[25] Further, π–π interactions between adjacent phenyl groups may drive more compact packing attract C_nOBCb molecules to in the surface monolayer.[24] Notably, the A_{cmc} value of $C_{18}OBCb$ is slightly larger than those of other homogeneous surfactants, which indicates that the hydrophobic tails are not vertical to the surface, likely resulting from coiling of the longer hydrophobic chains.[45,46]

The efficiency and effectiveness of surfactant adsorption at the air/water interface can be characterized by the logarithm of the surfactant concentration C_{20} at which the surface tension of water is reduced by 20 mN m^{-1} (pC_{20}) and by the cmc/C_{20} ratio,[47] respectively. The pC_{20} and cmc/C_{20} ratio values of C_n-OBCb are shown in Table 2 together with the data of C_nCb for comparison. The pC_{20} values of C_nOBCb increase as the hydrocarbon chain length increases from 12 to 16 and are larger than those of C_nCb with the same hydrocarbon chain lengths (pC_{20} = 3.91–5.54 (ref. 48)), suggesting that the C_nOBCb surfactants have a greater tendency to adsorb at air/water interface. However, for $C_{18}OBCb$, the pC_{20} value becomes smaller, possibly because of premicellar aggregation in solution. Further, the variation of the cmc/C_{20} ratio values of C_n-OBCb with the hydrocarbon chain length follows the same trend as the pC_{20} values, and the cmc/C_{20} ratio values of C_n-OBCb are approximately four times larger than those of C_nCb (cmc/C_{20} = 6.5–7.5 (ref. 48)). This finding suggests that it is more beneficial for C_nOBCb molecules to absorb at the air/water interface than to form micelles in the surfactant solution.

According to the single-stage equilibrium model, the standard free energy of micellization (ΔG^0_{mic}) and adsorption (ΔG^0_{ads}) for zwitterionic surfactants in aqueous solution can be calculated using the following equations:[49,50]

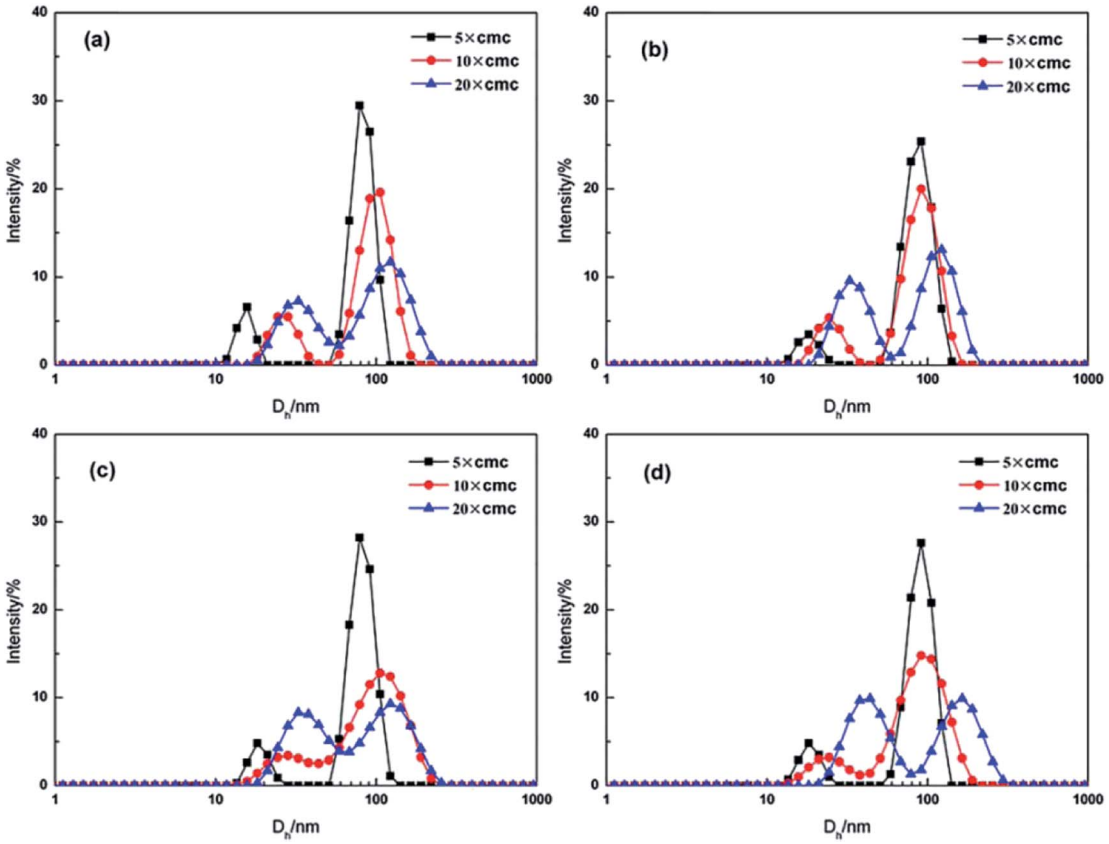

Fig. 6 Variation of size distribution with the surfactant concentration by DLS for C_nOBCb: n = (a) 12, (b) 14, (c) 16, (d) 18.

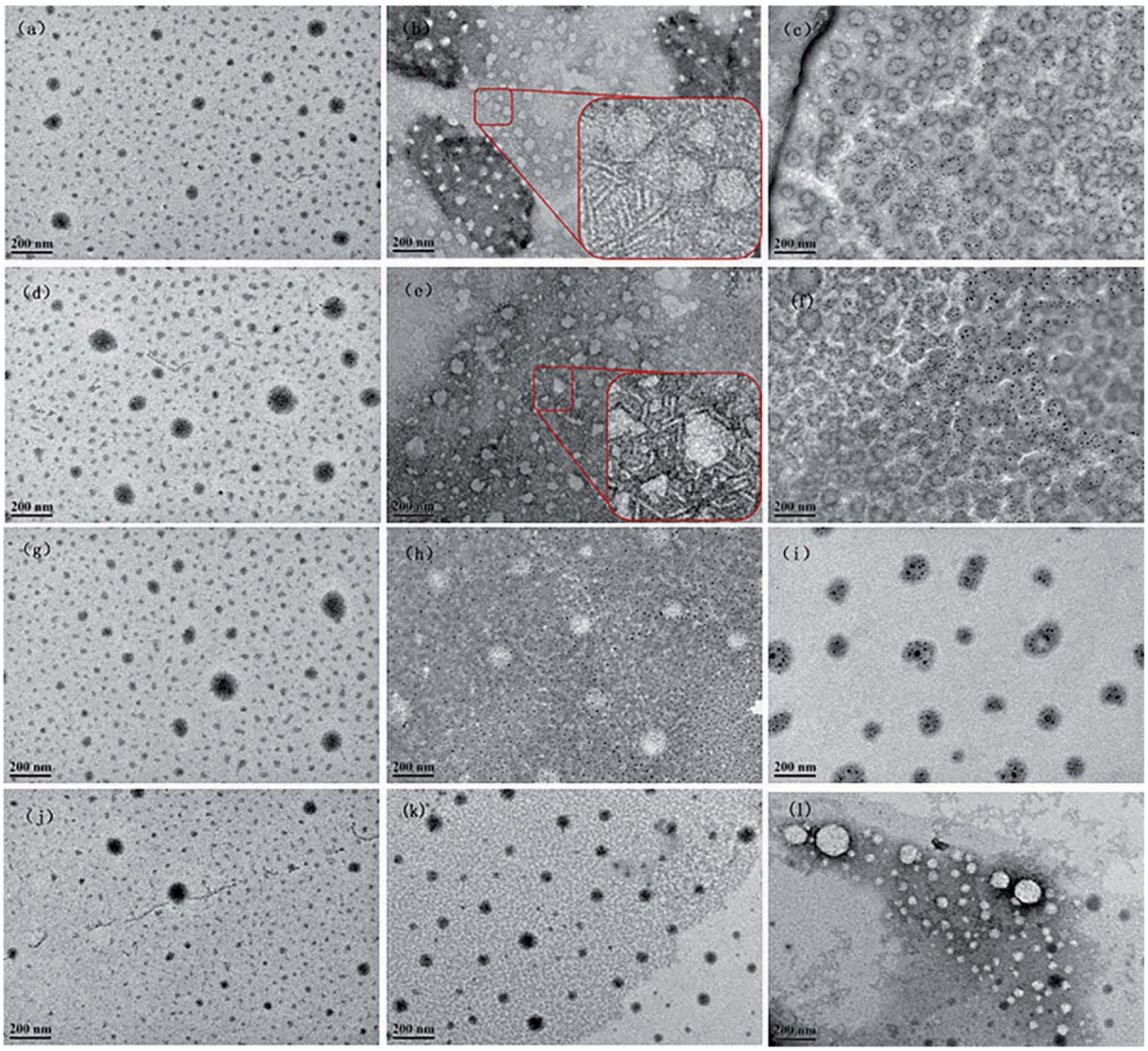

Fig. 7 TEM images of C_nOBCb ($n = 12$, 14, 16 and 18) aggregates: C_{12}OBCb at (a) 0.94 mmol dm^{-3} (5 × cmc), (b) 1.88 mmol dm^{-3} (10 × cmc), (c) 3.76 mmol dm^{-3} (20 × cmc); C_{14}OBCb at (d) 0.114 mmol dm^{-3} (5 × cmc), (e) 0.229 mmol dm^{-3} (10 × cmc), (f) 0.458 mmol dm^{-3} (20 × cmc); C_{16}OBCb at (g) 0.0115 mmol dm^{-3} (5 × cmc), (h) 0.023 mmol dm^{-3} (10 × cmc), (i) 0.046 mmol dm^{-3} (20 × cmc); C_{18}OBCb at (j) 0.0175 mmol dm^{-3} (5 × cmc), (k) 0.035 mmol dm^{-3} (10 × cmc), (l) 0.07 mmol dm^{-3} (20 × cmc).

$$\Delta G^0_{\mathrm{mic}} = RT \ln X_{\mathrm{cmc}} \quad (4)$$

$$\Delta G^0_{\mathrm{ads}} = \Delta G^0_{\mathrm{mic}} - \left(\frac{\gamma_0 - \gamma_{\mathrm{cmc}}}{\Gamma_{\mathrm{cmc}}}\right) \quad (5)$$

where R is the gas constant (8.314 J mol^{-1} K^{-1}), T is the absolute temperature, X_{cmc} is the cmc as a molar fraction (X_{cmc} = cmc/55.4), γ_0 and γ_{cmc} are the surface tensions of water and surfactant solution at the cmc, respectively. Because the micellization of C_nOBCb is a spontaneous process, the calculated $\Delta G^0_{\mathrm{mic}}$ values should be negative. The $\Delta G^0_{\mathrm{mic}}$ and $\Delta G^0_{\mathrm{ads}}$ values of C_nOBCb ($n = 12$, 14, 16, or 18) are tabulated in Table 2. Based on these results, the $\Delta G^0_{\mathrm{ads}}$ value of C_nOBCb is more negative than its $\Delta G^0_{\mathrm{mic}}$ value, signifying that the adsorption process is more favorable than micellization. This finding is also supported by the pC_{20} and cmc/C_{20} ratio values of C_nOBCb being larger than those of C_nCb. In addition, the negative values of $\Delta G^0_{\mathrm{mic}}$ and $\Delta G^0_{\mathrm{ads}}$ become larger on increasing the hydrocarbon chain length from 12 to 16, but are slightly smaller when the hydrocarbon chain length reaches 18. This phenomenon suggests that a driving force for micellization or adsorption is derived from the hydrophobic effect among hydrocarbon chains[51] and the deviation may be due to the stereo inhibition of the longer hydrocarbon chain.[36]

3.5. Micropolarity and micellization

The micropolarity and micellization of C_nOBCb ($n = 12$, 14, 16, or 18) were investigated using pyrene fluorescence and DLS measurements. In general, the scattering intensity obtained from DLS measurements increases as increasing the size and number of micelles increase. In fluorescence measurement, the I_1/I_3 ratio decreases from approximately 1.8 to 1.2 when micelles are formed, owing to the transfer of pyrene molecules from the

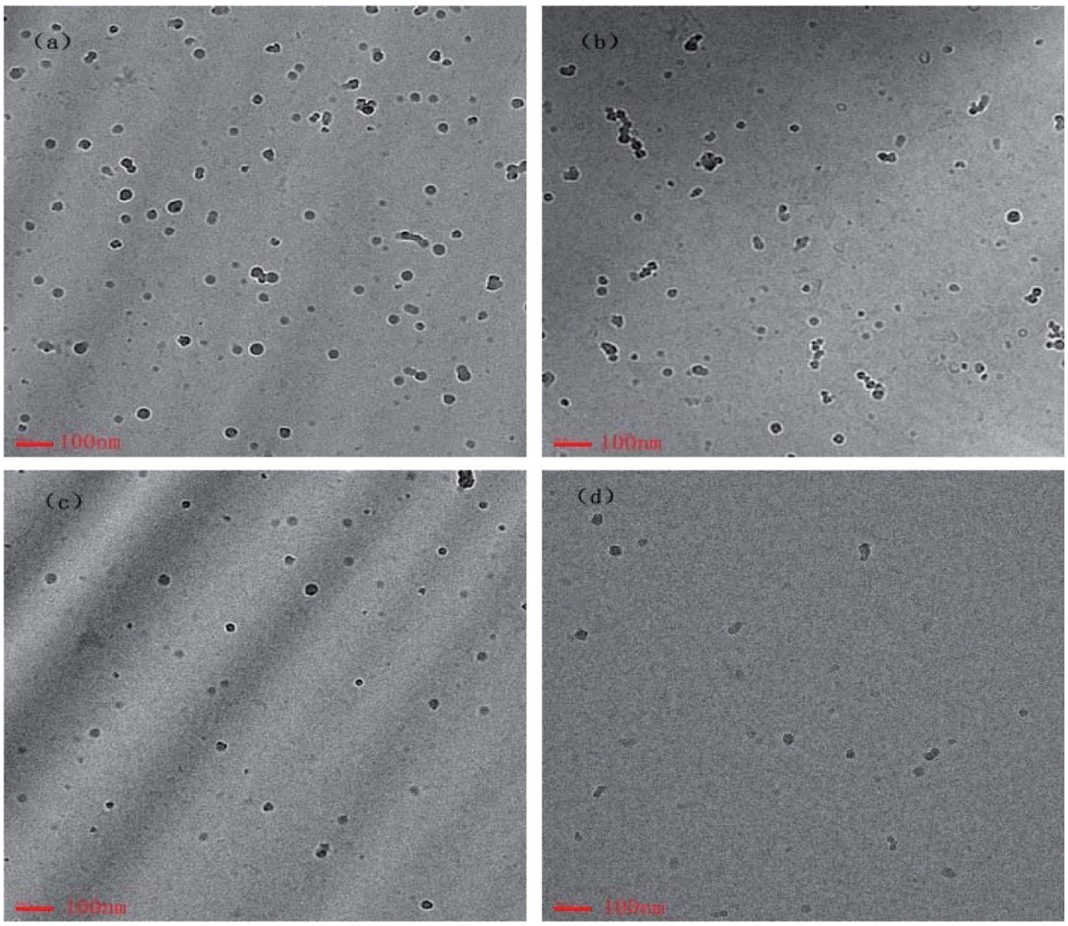

Fig. 8 Cryo-TEM images of vesicles formed at 20 × cmc for (a) C_{12}OBCb (3.76 mmol dm^{-3}), (b) C_{14}OBCb (0.458 mmol dm^{-3}), (c) C_{16}OBCb (0.046 mmol dm^{-3}), and (d) C_{18}OBCb (0.07 mmol dm^{-3}).

water environment into the interior hydrophobic region of micelles.[15] The variations of I_1/I_3 ratio (the fluorescence spectra of C_nOBCb are shown in the Fig. S13–S16†) and the scatting intensity as a function of C_nOBCb (n = 12, 14, 16, or 18) concentration are shown in Fig. 5. The I_1/I_3 ratio starts to decrease and the scattering intensity increases at a concentration close to the corresponding cmc. These results indicate that aggregates are formed at these concentrations in aqueous solution. Additionally, the I_1/I_3 ratios of C_nOBCb with n = 12, 14, 16 and 18 gradually decrease with increasing surfactant concentration. This trend is similar to the fluorescence results for heterogemini surfactants reported by Yoshimura *et al.*[36] who suggested that this phenomenon is probably due to a broad micelle size distribution. It is also worth noting that the minimum values of the I_1/I_3 ratio at high concentrations above the cmc are similar for the four C_nOBCb surfactants, suggesting that the hydrophobic length of the surfactant molecules has little effect on the I_1/I_3 ratio values. This result is also in good agreement with the behavior of conventional surfactants.[52,53]

3.6. Size and morphology of aggregates

To investigate the effect of the C_nOBCb concentration on the size and morphology of aggregates in aqueous solution, DLS and TEM measurements were performed. The apparent hydrodynamic diameters (D_h) for C_nOBCb (n = 12, 14, 16, or 18) were determined by DLS over a wide concentration range from 5 × cmc to 20 × cmc. As shown in Fig. 6, C_nOBCb show a bimodal distribution containing two peaks with a wide range of D_h values from 10 to 200 nm. As the light scattering intensity is proportional to the sixth power of the diameter of the particles, the major populations of aggregates are relatively small ones in the surfactant solution. The D_h values of aggregates of C_nOBCb (n = 12, 14, 16, or 18) slightly increase with increasing surfactant concentrations, which implies that the small aggregates existing at low surfactant concentrations can gradually transform into large aggregates as the surfactant concentration increases. This trend is similar to the results obtained for sulfatebetaine zwitterionic gemini surfactants.[54]

To directly visualize of the morphologies of the C_nOBCb aggregates, TEM measurements were conducted at the concentrations used for DLS measurements. TEM images of C_nOBCb at different concentrations (Fig. 7) clearly exhibit the presence of closed vesicles in aqueous solution. The vesicles size determined from TEM measurements are consistent with the DLS results. For C_{12}OBCb and C_{14}OBCb, predominant small spherical micelles and several large vesicles with average diameter about 15 and 80 nm, respectively, were observed at low concentrations (5 × cmc) (Fig. 7(a) and (d)). On further

Table 3 Core parameters and EOR of $C_{12}Cb$ and C_nOBCb (n = 12, 14, 16, 18)

Core no.	Length (cm)	Diameter (cm)	Porosity (%)	Permeability (mD)	Sample (0.5 mmol dm^{-3})	E_1 (%)	E_2 (%)	EOR (%)
1#	7.162	2.520	26.45	132.65	$C_{12}Cb$	48.54	55.27	6.73
2#	7.228	2.524	25.82	126.46	$C_{12}OBCb$	48.89	59.44	10.55
3#	7.218	2.518	26.15	134.60	$C_{14}OBCb$	47.03	56.11	9.08
4#	7.224	2.516	25.87	137.22	$C_{16}OBCb$	48.49	57.73	9.24
5#	7.216	2.520	25.80	134.81	$C_{18}OBCb$	48.41	56.26	7.85

increasing the surfactant concentration to 10 × cmc, the small micelles grow into partially elongated vesicles and larger spherical vesicles (Fig. 7(b) and (e)), consistent with the higher polydisperse index (PDI) value obtained by DLS. The elongated vesicles are 50–80 nm long with diameters of 5 nm. The growth of spherical micelles into partially elongated micelles has been reported for ionic liquids containing an imidazolium ring,[54] this may be caused by the stronger hydrophobicity imparted by the presence of a phenyl group within the long hydrocarbon chain. When the concentration increases to 20 × cmc, the sizes of the small and large vesicles are centered at 35 and 110 nm, respectively. Surprisingly, the formation of elongated vesicles was not observed in for $C_{16}OBCb$ and $C_{18}OBCb$ (Fig. 7(h) and (k)), and only spherical micelles or elliptical vesicles were formed within the investigated concentration ranges. The Cryo-TEM experiments for C_nOBCb (n = 12, 14, 16, 18) at the concentrations of 20 × cmc were carried out and the Cryo-TEM images were shown in Fig. 8. The formation of spherical particles was also observed for all of these four surfactants from cryo-TEM images whose dimension matches closely with DLS and TEM data.

Moreover, optical microscope by OLYMPUS BX51 Fluorescence Microscopy was performed to investigate encapsulation ability of this new class of surfactants. The fluorescent image for $C_{12}OBCb$ solution (3.76 mmol dm^{-3}) dyed with calcein is shown in Fig. S17.† It can be seen that calcein was well encapsulated into the vesicles. The diameter of small vesicles is a few tens of nanometers, which is also consistent with the DLS and TEM results.

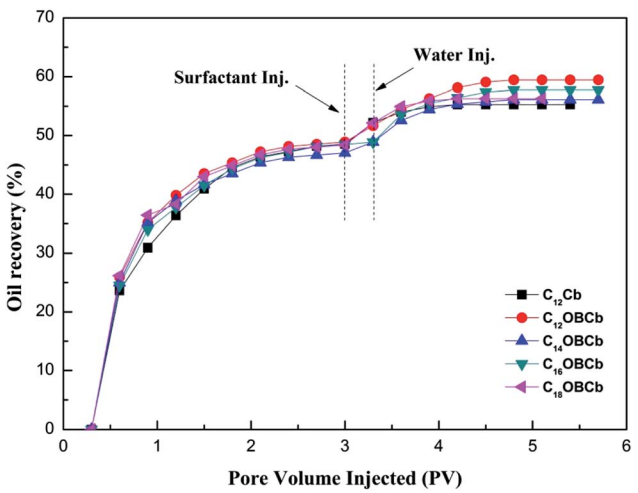

Fig. 9 Oil recovery as a function of pore volume injected (PV) for $C_{12}Cb$ and C_nOBCb (n = 12, 14, 16, 18).

3.6. Core flooding experiment

The capability of enhancing oil recovery for the $C_{12}Cb$ and C_n-OBCb (n = 12, 14, 16, 18) solution was evaluated in sandstone core, and the results of the surfactant flood ing were summarized in Table 3. The displacement efficiency of C_nOBCb (n = 12, 14, 16, 18) is slightly higher than that of $C_{12}Cb$ (6.73%) at the same surfactant concentration (Fig. 9). $C_{12}OBCb$ enhanced an additional oil recovery of 10.55%, which was the highest among the C_nOBCb species. The relatively higher oil recovery for C_n-OBCb surfactants could be attributed to the excellent interfacial tension properties.

4. Conclusions

A novel series of phenyl-containing carboxybetaine surfactants were successfully prepared by an efficient and high-yield synthesis route and characterized by ^{1}H NMR, ^{13}C NMR, and ESI-HRMS. The TGA results showed that C_nOBCb was stable and difficult to decompose below 200 °C. C_nOBCb exhibited superior surface activities, including lower cmc (0.1881–0.0023 mmol dm^{-3}), higher efficiency in lowering the surface tension of water (25.6–32.6 mN m^{-1}) and stronger adsorption tendency at the air/water interface, in comparison with C_nCb with the same hydrocarbon chain length. C_nOBCb also showed excellent interfacial tension activity against toluene, with $C_{12}OBCb$ reaching ultralow interfacial tension (10^{-3} mN m^{-1}) in the range of 0.2–1 mmol dm^{-3}. The DLS and TEM results showed that the C_nOBCb could spontaneous aggregate into vesicles, and the sizes of the aggregates increase with increasing surfactant concentrations. In particular, C_nOBCb with n = 12 and 14 aggregated to form elongated micelles at 10 × cmc. From these results, it could be concluded that the presence of a phenyl group in the hydrophobic chain has a dramatic effect on the surface–active properties and aggregation behavior of betaine-type surfactants. Moreover, core flooding experiments directly demonstrate that C_nOBCb could remarkably enhance oil recovery by 7.85–10.55%.

Conflicts of interest

There are no conflicts to declare.

Acknowledgements

We are grateful for the financial supports from the National Natural Science Foundation of China (Grants No. 51474223).

References

1 V. Seredyuk, E. Alami, M. Nydén and K. Holmberg, *Langmuir*, 2001, **17**, 5160–5165.
2 K. Singh and D. G. Marangoni, *J. Colloid Interface Sci.*, 2007, **315**, 620–626.
3 D. Wieczorek, A. Dobrowolski, K. Staszak, D. Kwaśniewska and P. Dubyk, *J. Surfactants Deterg.*, 2017, **20**, 151–158.
4 S. S. Hu, L. Zhang, Z. C. Xu, Q. T. Gong, Z. Q. Jin, L. Luo, L. Zhang and S. Zhao, *Appl. Surf. Sci.*, 2015, **355**, 868–877.
5 B. L. Song, X. Hu, X. Q. Shui, Z. G. Cui and Z. J. Wang, *Colloids Surf., A*, 2016, **489**, 433–440.
6 Z. G. Cui, D. Qi, B. l. Song, X. M. Pei and X. Hu, *Energy Fuels*, 2016, **30**, 2043–2051.
7 S. Alzobaidi, C. Da, V. Tran, M. Prodanović and K. P. Johnston, *J. Colloid Interface Sci.*, 2017, **488**, 79–91.
8 T. Tamuraa, T. Iiharab, S. Nishidab and S. Ohtab, *J. Surfactants Deterg.*, 1997, **2**, 207–211.
9 I. Bozetine, T. A. Zaïd, C. E. Chitour and J. P. Canselier, *J. Surfactants Deterg.*, 2008, **11**, 299–305.
10 R. Mostafalul, A. Banaei and F. Ghorbani, *J. Surfactants Deterg.*, 2015, **15**, 919–922.
11 N. C. Christov, N. D. Denkov, P. A. Kralchevsky, K. P. Ananthapadmanabhan and A. Lips, *Langmuir*, 2004, **20**, 565–571.
12 B. L. Song, X. Hu, X. Q. Shui, Z. G. Cuia and Z. J. Wang, *Colloids Surf., A*, 2016, **489**, 433–440.
13 V. T. Kelleppan, J. E. Moore, T. M. McCoy, A. V. Sokolova, L. de Campo, B. L. Wilkinson and R. F. Tabor, *Langmuir*, 2018, **34**, 970–977.
14 K. Nyuta, T. Yoshimura and K. Esumi, *J. Colloid Interface Sci.*, 2006, **301**, 267–273.
15 T. Yoshimura, T. Ichinokawa, M. Kaji and K. Esumi, *Colloids Surf., A*, 2006, **273**, 208–212.
16 J. H. Zhao, C. L. Dai, Q. F. Ding, M. Y. Du, H. S. Feng, Z. Y. Wei, A. Chen and M. W. Zhao, *RSC Adv.*, 2015, **5**, 13993–14001.
17 L. Y. Hou, H. N. Zhang, H. Chen, Q. B. Xia, D. Y. Huang, L. Meng and X. F. Liu, *J. Surfactants Deterg.*, 2013, **17**, 403–408.
18 M. Zhou, G. Luo, Z. Zhang, S. S. Li and C. W. Wang, *J. Mol. Struct.*, 2017, **1144**, 199–205.
19 D. Wieczorek, A. Dobrowolski, K. Staszak, D. Kwasniewska and P. Dubyk, *J. Surfactants Deterg.*, 2017, **10**, 151–158.
20 R. A. Khalil and F. A. Saadoon, *J. Saudi Chem. Soc.*, 2015, **19**, 423–428.
21 V. K. Sharma, S. Mitra, M. Johnson and R. Mukhopadhyay, *J. Phys. Chem. B*, 2013, **117**, 6250–6255.
22 V. I. Martín, A. Rodríguez, M. M. Graciani, I. Robina, A. Carmona and M. L. Moyá, *J. Colloid Interface Sci.*, 2011, **363**, 284–294.
23 Y. J. Li, J. Reeve, Y. L. Wang, R. K. Thomas, J. B. Wang and H. K. Yan, *J. Phys. Chem. B*, 2005, **109**, 16070–16074.
24 K. Taleb, M. Mohamed-Benkada, N. Benhamed, S. Saidi-Besbes, Y. Grohens and A. Derdour, *J. Mol. Liq.*, 2017, **241**, 81–90.
25 M. A. Hegazy, M. Abdallah and H. Ahmed, *Corros. Sci.*, 2010, **52**, 2897–2904.
26 Q. Zhang, M. Z. Tian, Y. C. Han, C. X. Wu, Z. B. Li and Y. L. Wang, *J. Colloid Interface Sci.*, 2011, **362**, 406–414.
27 S. De, V. K. Aswal and S. Ramakrishnan, *Langmuir*, 2010, **26**, 17882–17889.
28 S. S. Hu, Z. H. Zhou, L. Zhang, Z. C. Xu, Q. T. Gong, Z. Q. Jin, L. Zhang and S. Zhao, *Soft Matter*, 2015, **11**, 7960–7968.
29 Z. Y. Liu, Z. C. Xu, H. Zhou, Y. L. Wang, Q. Liao, L. Zhang and S. Zhao, *J. Mol. Liq.*, 2017, **240**, 412–419.
30 Q. Q. Zhang, B. X. Cai, H. Z. Gang, S. Z. Yang and B. Z. Mu, *RSC Adv.*, 2014, **4**, 38393–38396.
31 L. F. Dong, X. L. Cao, Z. Q. Li, L. Zhang, Z. C. Xu, L. Zhang and S. Zhao, *Colloids Surf., A*, 2014, **444**, 257–268.
32 M. J. Rosen, A. W. Cohen, M. Dahanayake and X. Y. Hua, *J. Phys. Chem.*, 1982, **86**, 541–545.
33 V. Seredyuk, E. Alami, M. Nydén and K. Holmberg, *Langmuir*, 2001, **17**, 5160–5165.
34 K. Kalyanasundaram and J. K. Thomas, *J. Am. Chem. Soc.*, 1977, **99**, 2039–2044.
35 J. X. Shen, Y. Y Bai, Q. W. Yin, W. X. Wang, X. Y Ma and G. Y Wang, *J. Ind. Eng. Chem.*, 2017, **56**, 82–89.
36 T. Yoshimura, K. Nyuta and K. Esumi, *Langmuir*, 2005, **21**, 2682–2688.
37 H. B. Klevens, *J. Phys. Colloid Chem.*, 1948, **52**, 130–148.
38 F. M. Menger, J. S. Keiper and V. Azov, *Langmuir*, 2000, **16**, 2062–2067.
39 M. J. Rosen, J. H. Mathias and L. Davenport, *Langmuir*, 1999, **15**, 7340–7346.
40 P. Mukerjee, *Adv. Colloid Interface Sci.*, 1967, **1**, 242–275.
41 J. G. Weers, J. F. Rathman, F. U. Axe, C. A. Crichlow, L. D. Foland, D. R. Scheuing, R. J. Wiersema and A. G. Zielske, *Langmuir*, 1991, **7**, 854–867.
42 J. Hoque, P. Akkapeddi, V. Yarlagadda, D. S. Uppu, P. Kumar and J. Haldar, *Langmuir*, 2012, **28**, 12225–12234.
43 D. Feng, Y. M. Zhang, Q. S. Chen, J. Y. Wang, B. Li and Y. J. Feng, *J. Surfactants Deterg.*, 2012, **15**, 657–661.
44 F. M. Menger and C. A. Littau, *J. Am. Chem. Soc.*, 1993, **115**, 10083–10090.
45 B. Li, Q. Zhang, Y. Xia and Z. N. Gao, *Colloids Surf., A*, 2015, **470**, 211–217.
46 L. M. Zhou, X. H. Jiang, Y. T. Li, Z. Chen and X. Q. Hu, *Langmuir*, 2007, **23**, 11404–11408.
47 M. Q. Ao, G. Y. Xu, Y. Y. Zhu and Y. Bai, *J. Colloid Interface Sci.*, 2008, **326**, 490–495.
48 M. J. Rosen and J. T. Kunjappu, *Surfactants and interfacial phenomena*, Surfactants and interfacial phenomena, 4th edn, 2012. pp. 93–94.
49 X. Q. Wang, J. Liu, L. Yu, J. J. Jiao, R. Wang and L. M. Sun, *J. Colloid Interface Sci.*, 2013, **391**, 103–110.
50 Y. Chevalier, Y. Storet, S. Pourchet and P. L. Perchec, *Langmuir*, 1991, **7**, 848–853.

51 T. Yoshimura and K. Esumi, *J. Colloid Interface Sci.*, 2004, **276**, 231–238.
52 K. Sakai, S. Umezawa, M. Tamura, Y. Takamatsu, K. Tsuchiya, K. Torigoe, T. Ohkubo, T. Yoshimura, K. Esumi, H. Sakai and M. Abe, *J. Colloid Interface Sci.*, 2008, **318**, 440–448.
53 B. Cai, X. F. Li, Y. Yang and J. F. Dong, *J. Colloid Interface Sci.*, 2012, **370**, 111–116.
54 G. Singh, G. Singh and T. S. Kang, *J. Phys. Chem. B*, 2016, **120**, 1092–1105.